Vietnam Journal of Mechanics, Vol. 48, No. 2 (2026), pp. 120 – 140
DOI: https://doi.org/10.15625/0866-7136/23483

THERMOACOUSTIC MODELING OF NONLOCAL CYLINDRICAL RODS VIA MEMORY-DEPENDENT DERIVATIVES

Jitendra Patil[1], **Chandrakant Jadhav**[2], **Nitin Chandel**[3,*], **Vinod Varghese**[4]
[1]*Department of Mathematics, S.S.V.P.S. Arts, Commerce and Science College, Shindkheda, Dhule, India*
[2]*Department of Mathematics, S.V.S. Dadasaheb Rawal Arts and Science College, Dondaicha, Dhule, India*
[3]*Department of Mathematics, Priyadarshini College of Engineering, Nagpur, India*
[4]*Department of Mathematics, M.G. College, Armori, Gadchiroli, India*
E-mail: nitinsinghchandel9@gmail.com

Received: 22 September 2025 / Revised: 21 October 2025 / Accepted: 28 October 2025
Published online: 8 June 2026

Abstract. This research investigates the application of a memory-dependent derivative (MDD) framework, utilizing diverse memory kernels to analyze thermoacoustic behaviors in media and materials affected by sound wave propagation. In solids such as copper, acoustic pressure significantly affects mechanical properties such as stress and deformation. By employing an advanced single-phase-lag (SPL) model, the study incorporates modern thermal conduction dynamics and nonlocal stress phenomena, effectively capturing delayed heat conduction and stress propagation for deeper insights into wave dynamics and material deformation. The research examines the effects of acoustic pressure on a cylindrical rod exposed to a moving Heaviside-type heat source, offering a detailed understanding of the interactions among thermal responses, mechanical elasticity, and acoustic wave propagation. For the Fourier series inversion method applied to numerical Laplace transform inversion, copper is selected as the representative material for computational simulations. The findings hold great promise for optimizing advanced material designs in acoustic and thermal systems, paving the way for next-generation smart materials and adaptive technologies that meet sustainable, high-performance requirements.

Keywords: single-phase-lag, heat conduction, thermal stresses, thermoelastic, cylindrical rod, acoustic, thermal shock, nonlocal.

NOTATION

Symbol	Description	SI Unit
T	Thermodynamic Temperature	K (kelvin)
T_0	Reference temperature	K (kelvin)
q	Heat conduction vector	W/m^2
k	Thermal conductivity coefficient	W/(m·K)
C_e	Specific heat capacity	J/(kg·K)
τ_q	Phase lag of heat flux	s (second)
τ_η	Phase lag of diffusing mass	s (second)
ϕ	Chemical potential	J/mol
c_s	Speed of sound in material	m/s
λ, μ	Lamé's constants	Pa (pascal)

Symbol	Description	SI Unit
∇^2	Laplacian operator	m^{-2}
σ_{ij}	Components of the stress tensor	Pa (pascal)
ε_{ij}	Components of strain tensor	dimensionless
ρ	Density (assumed time-independent)	$\mathrm{kg/m}^3$
C	Concentration of diffusing mass	$\mathrm{mol/m}^3$
$\mathfrak{D}$	Diffusion coefficient	m^2/s
α_c	Linear diffusion coefficient	m^2/s
η	Flow of diffusing mass vector	$\mathrm{mol/(m}^2\cdot\mathrm{s)}$
δ_{ij}	Kronecker delta function	dimensionless
α_t	Thermal expansion factor	1/K
$\alpha_1 = (3\lambda + 2\mu)\alpha_t$	Thermal coupling parameter	dimensionless or $\mathrm{J/(m}^3\cdot\mathrm{K)}$
$\alpha_2 = (3\lambda + 2\mu)\alpha_c$	Diffusion coupling parameter	dimensionless or $\mathrm{J/(m}^3\cdot\mathrm{mol)}$
$H(t)$	Heaviside function of time	dimensionless
s	Laplace parameter	1/s
a	Measure of diffusive effect	m^2/s
b	Measure of thermo-diffusion effect	dimensionless or $\mathrm{J/(m}^3\cdot\mathrm{K}\cdot\mathrm{mol)}$

1. INTRODUCTION

The study of thermo-diffusion models has gained significant attention due to their critical role in understanding the interplay between thermal, mechanical, and acoustic phenomena in various materials (Atta et al., 2024). Among these, the influence of acoustic pressure and nonlocal stress effects has emerged as a key area of research, particularly in the context of advanced materials such as copper. These materials exhibit unique responses to external stimuli, such as heat and mechanical forces, making them ideal candidates for exploring complex wave dynamics and deformation behaviors. Thermoelasticity, a field that examines the coupling between thermal and elastic effects, has evolved significantly since its inception. Classical thermoelastic theories, which are based on Fourier's law of heat conduction, have been widely used to model heat transfer and stress propagation. However, these models are limited by the assumption of infinite heat conduction speed, which is physically unrealistic. Generalized thermoelastic theories that incorporate non-Fourier heat conduction models have been developed to address this limitation. These advancements include the introduction of phase-lag models, such as the single-phase-lag (SPL) model, which accounts for the finite speed of heat conduction and provides a more accurate representation of thermal and mechanical interactions (Shakeriaski et al., 2021).

Fractional calculus is a mathematical framework that extends differentiation and integration to non-integer orders, offering a more detailed understanding of complex phenomena in fields such as heat conduction, diffusion processes, and electromagnetism (Galucio et al., 2004; Jesus & Machado, 2009; Kilbas et al., 2006; Mainardi, 1996; Meral et al., 2010; Podlubny, 1990). It is increasingly used in science, engineering, and applied mathematics to describe fundamental physical phenomena in complex materials. Researchers have developed methods to solve fractional differential equations using fractional operators, including Hilfer, Caputo, and Riemann-Liouville (Atangana & Gómez-Aguilar, 2018; Furati et al., 2012; Veeresha et al., 2019), to enhance the accuracy of these solutions. Podlubny (1990) offers an in-depth exploration of fractional calculus applications in science and engineering, while Miller and Ross (1993) provide a foundational book with a comprehensive historical perspective. Borino et al. (2011) emphasize the importance of long-range heat flow and a modified Fourier heat flux equation, presenting a physical interpretation of fractional and nonlocal phenomena in heat conduction.

The recently introduced concept of memory-dependent derivatives (MDD) expands the standard derivative into an integral form with a kernel function over a sliding interval (Wang & Li, 2011). This inclusion of memory enhances its applicability beyond fractional differentiation. Memory-dependent effects, prevalent in various physical phenomena, indicate that a system's current state depends not only on its location and time but also on its past states. The integration of memory-dependent derivatives (MDD) into thermoelastic models has further enhanced their applicability by capturing the delayed effects of heat conduction and stress propagation. MDD frameworks, combined with diverse memory kernels, enable a more comprehensive understanding of material behavior under dynamic conditions. Researchers have explored their integration into various thermoelastic theories, such as generalized thermoelasticity (Yu et al., 2014), magneto-thermoelasticity (Ezzat et al., 2015), and electro-thermoelasticity (Ezzat et al., 2016). These studies introduce innovative approaches to account for past stress, strain, and heat transfer states, thereby enhancing the accuracy of predictions for material responses. Applications extend to dynamic scenarios, including nonlocal rotating thermoelastic half-spaces (Said, 2022) and thermo-piezoelectric functionally graded rotating rods (Abouelregal et al., 2023). Mondal (2020) has demonstrated the significance of MDD in magneto-thermoelastic systems under nonlocal dual-phase lag heat conduction. Recently, Chandel et al. (2024) conducted a nonlocal thermoelastic analysis of a spherically symmetric elastic sphere considering memory effects, providing valuable insights into spherically symmetric systems. Dhore et al. (2025) investigated the hygrothermoelastic behavior of nano-circular plates incorporating memory effects, addressing the intricate coupling between thermal, moisture, and elastic fields in nanoscale structures. Balwir et al. (2024) focused on the memory response in quasi-static thermoelastic stress within a rod subjected to distributed time-dependent heat sources, offering a detailed exploration of time-varying thermal influences. Additionally, Chandel, Khalsa, and Varghese (2025) examined nonsimple thermoelastic diffusion interactions in a half-space under nonlocality and memory effects, contributing to the broader understanding of diffusion phenomena in nonsimple materials. These works collectively aim to refine theoretical models, enabling deeper insights into material behaviors in complex engineering contexts.

Nonlocal theory, a cornerstone in solid-state physics, posits that the state of each point within a material influences its neighboring particles — a principle vital for explaining material properties at small scales. The foundational work of Eringen and Edelen (Eringen & Edelen, 1972) introduced nonlocal elasticity, a framework that integrates atomic interactions into macroscopic models. Eringen's subsequent contributions (Eringen, 1974a, 1974b, 1984) extended this theory, laying the foundation. Stress-driven nonlocal methodologies, as reviewed by Barretta et al. (2023), have provided insights into size-dependent static and dynamic behaviors in nanostructures, bridging the gap between theory and nanotechnology. Ghavanloo et al. (2019) explored comprehensive applications of nonlocal elasticity models for nanoscopic structures, highlighting their versatility. Moreover, Abouelregal (2024) introduced fractional derivatives into Eringen's nonlocal thermoelastic framework, advancing the modeling of generalized thermoelastic materials. These developments underscore the significance of nonlocal theory in capturing complex physical phenomena in advanced engineering and material science.

Recently, the modified nonlocal Klein-Gordon operator has provided a sophisticated mathematical framework to describe thermoelastic fields, accounting for spatial and temporal nonlocality. This approach introduces two critical parameters: the characteristic internal length scale due to spatial nonlocality and the characteristic time scale due to temporal nonlocality, both represented by positive real numbers. These parameters offer a nuanced understanding of material behavior in systems where interactions extend beyond immediate neighboring particles. Lazar and Lazar and Agiasofitou (2022) explored the fundamentals of nonlocal elasticity of the Klein-Gordon type, presenting its applications in wave propagation phenomena. In a recent study, Chandel et al. (2024) presented comprehensive applications of the nonlocality

framework, grounded in the Klein-Gordon nonlocality stress theory, which has been utilized to predict the thermoelastic behavior of materials under extreme environmental conditions. Their study emphasizes the operator's significance in advancing nonlocal theories and modeling complex physical fields, thus contributing to the broader understanding of dynamic responses in materials.

This study focuses on the impact of acoustic pressure and nonlocality on thermo-diffusion models with memory effects. By employing an innovative SPL model, the research aims to analyze the thermoelastic response of materials such as copper subjected to a moving Heaviside-type heat source. The Fourier series inversion approach allows the numerical inversion of the Laplace transform, facilitating a detailed examination of wave dynamics and material deformation. These findings have potential applications in optimizing the design and performance of advanced materials for acoustic and thermal systems, as well as in the development of next-generation smart materials and adaptive technologies. Although the rod geometry is macroscale, the excitation wavelengths lie in the microscale regime, necessitating a nonlocal elasticity framework to capture size-dependent stress propagation.

The manuscript is organized as follows: Section 2 introduces a novel mathematical model incorporating nonlocal space-time lag characteristics, resulting in an advanced framework for analyzing thermoelastic behavior in materials. Section 3 presents the problem formulation and an analysis of the interplay among thermal, mechanical-elastic, and acoustic wave propagation in a solid material, such as a cylindrical rod, under a moving Heaviside-type heat source. In Section 4, the solution methodology utilizes the Laplace transform technique via the operational method, converting differential equations into algebraic expressions for efficient analysis. Section 5 details the numerical inversion of the Laplace transform, performed using the Fourier series expansion technique. Section 6 provides numerical results, accompanied by a detailed analysis and commentary on temperature, displacement, stress, and strain distributions. Finally, Section 7 summarizes the key findings and contributions of the study, facilitating a rigorous exploration of memory effects and nonlocal dynamics in solids.

2. MATHEMATICAL MODELING

The development of thermoelasticity theory grounded in Fourier's law can be credited to the work of Biot (1956). However, the classical theory faced a significant limitation due to its reliance on Fourier's equation $q(x,t) = -k\,\nabla T(x,t)$, which assumes an infinite speed of heat conduction, which is an unrealistic physical scenario. This shortcoming led to the emergence of non-Fourier heat conduction models, which formed the foundation of generalized thermoelastic theories. These advancements were implemented through various methods, including introducing phase lags, adding consecutive variables, modifying equations, and incorporating nonlocal effects. Lord and Shulman (1967) addressed the issue of infinite thermal wave speed by adopting the heat conduction model proposed by Cattaneo (1958) and Vernotte (1958) . This approach incorporated a relaxation parameter associated with the heat flux vector into Fourier's law, significantly improving the thermoelasticity theory with a non-Fourier equation $(1+\tau_0(\partial/\partial t))q(x,t) = -k\,\nabla T(x,t)$. The revised model introduced modifications to describe heat transfer more realistically. Moreover, both spatially nonlocal and temporally lagging behaviors have been recognized as integral aspects of this theory, particularly evident in microscale heat transport phenomena (Tzou, 2014). The heat conduction equation is given by (Cattaneo, 1958; Lord & Shulman, 1967; Vernotte, 1958)

$$q(x+\ell, t+\tau_q) = -k\,\nabla T(x,t), \tag{1}$$

where ℓ is the correlation or nonlocal length vector. By Taylor series expansion

$$q(x,t) + (\ell\cdot\nabla)q(x,t) + \tau_q\frac{\partial q}{\partial t} = -k\nabla T. \tag{2}$$

The energy equation can be formulated as

$$\rho\, C_e \frac{\partial T}{\partial t} + \alpha_1 T_0 \frac{\partial}{\partial t}(div\, u\,) + aT_0 \frac{\partial C}{\partial t} = -div\, \vec{q} + Q. \tag{3}$$

The mass diffusion equation is given as

$$\eta(x,t) = -\mathcal{D}\,\nabla\phi(x,t). \tag{4}$$

For lagging behavior, the generalized constitutive equation for diffusion is proposed as

$$\eta(r, t+\tau_\eta) = -\mathcal{D}\,\nabla\phi(x,t). \tag{5}$$

By Taylor series expansion, the diffusion Eq. (5) is

$$\left(1 + \tau_\eta \frac{\partial}{\partial t}\right)\eta = -\mathcal{D}\,\nabla\phi. \tag{6}$$

The chemical potential and mass conservation equation are as follows

$$\phi = -\alpha_2 e + bC - aT, \tag{7}$$

$$\nabla \cdot \eta = -\frac{\partial C}{\partial t}. \tag{8}$$

Taking the divergence of both sides of Eqs. (2) and (6) and using Eqs. (3) and (7)–(8) yields

$$\left(1 + \ell\frac{\partial}{\partial x} + \tau_q \frac{\partial}{\partial t}\right)\left(\rho\, C_e \frac{\partial T}{\partial t} + \alpha_1 T_0 \frac{\partial}{\partial t}(div\, u\,) + aT_0 \frac{\partial C}{\partial t} - Q\right) = k\nabla^2 T, \tag{9}$$

$$\left(1 + \tau_\eta \frac{\partial}{\partial t}\right)\frac{\partial C}{\partial t} = \mathcal{D}[-\alpha_2 \nabla^2 e + b\nabla^2 C - a\nabla^2 T], \tag{10}$$

where $\tau_q \geqslant 0$.

A material's behavior under acoustic pressure is influenced by its physical properties, such as density, elasticity, and structural arrangement. These features make the study of acoustic pressure useful for various applications, including material characterization and structural health monitoring. Related phenomena are represented mathematically by the following equation (Chandel, Khalsa, Abouelregal, et al., 2025; El-Dali et al., 2024; Raddadi et al., 2025)

$$\nabla^2 \mathcal{P} - \frac{1}{c_s^2}\frac{\partial^2 \mathcal{P}}{\partial t^2} = \zeta\beta \frac{\partial^2 T}{\partial t^2}. \tag{11}$$

The acoustic wavelength, derived from excitation frequency and material properties, falls within the microscale regime, reinforcing the need for nonlocal stress modeling. Here, ζ and β denote an adiabatic index or specific heat ratio and a volumetric thermal expansion coefficient, respectively.

The nonlocal stress constitutive equation is given by (Sur, 2024)

$$(1 - \varepsilon^2\nabla^2)\sigma_{ij} = 2\mu e_{ij} + \lambda e\delta_{ij} - \alpha_1 T\delta_{ij} - \alpha_2 C\delta_{ij}. \tag{12}$$

This nonlocal stress formulation follows Eringen's theory (Eringen, 1974a, 1974b, 1984; Eringen & Edelen, 1972) and the Klein–Gordon-type extension by Lazar and Agiasofitou (2022). This approach is essential when the characteristic wavelength of acoustic or thermal excitation becomes comparable to the structural dimensions, as is the case in microscale thermoelastic systems. The model captures both spatial and temporal nonlocality, allowing for a more realistic representation of stress dispersion and wave-structure interaction under memory-dependent excitation.

The strain-displacement relation equation

$$e_{ij} = (u_{i,j} + u_{j,i})/2. \tag{13}$$

The equilibrium equation, in the absence of any external body forces, is given as follows

$$\sigma_{ji,j} = \rho\,(\partial^2 u_i/\partial t^2). \tag{14}$$

Substituting Eqs. (12) and (13) into Eq. (14) yields

$$(1-\varepsilon^2\nabla^2)\rho\,(\partial^2 u_i/\partial t^2) = (\lambda+\mu)u_{j,ij} + \mu u_{i,ij} - \alpha_1 T_i - \alpha_2 C_i. \tag{15}$$

3. PROBLEM FORMULATION AND ANALYSIS

Consider a thermoelastic thin cylindrical rod of length L as shown in Fig. 1, with a reference temperature T_0. The rod is fixed at both ends and subjected to a heat source that moves along its length. The rod is subjected to thermal shock $T_1 H(t)$ and chemical potential shocks $\phi_1 H(t)$ from the origin. The other end of the rod is thermally insulated, as in Fig. 1. The dynamic problem of the thermoelastic thin rods can be considered one-dimensional, based on the assumption that the longitudinal scale along the x-axis significantly exceeds the scales in the other two perpendicular directions.

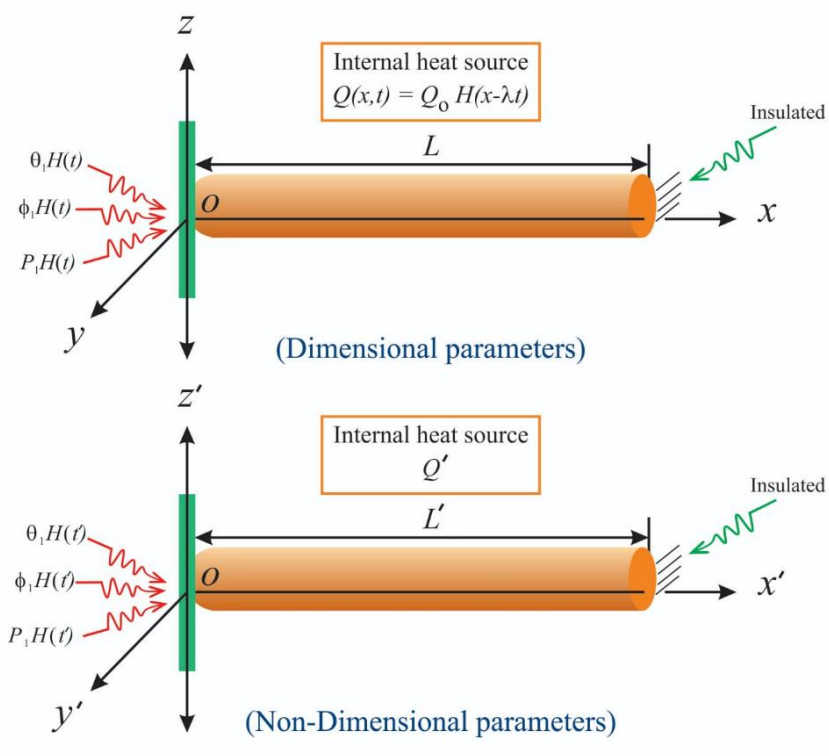

Fig. 1. Schematic of a finite-length rod with sectional sources

3.1. Thermal stress

The basic equation in one-dimensional form

$$(1-\varepsilon^2\nabla^2)\sigma_{xx} = (\lambda+2\mu)\,\frac{\partial u}{\partial x} - \alpha_1 T - \alpha_2 C. \tag{16}$$

The cubical dilation

$$e = div\,u = \partial u/\partial x. \tag{17}$$

From Eqs. (12)–(15), we obtain

$$(\lambda+2\mu)\frac{\partial e}{\partial x} - \alpha_1\frac{\partial T}{\partial x} - \alpha_2\frac{\partial C}{\partial x} = \rho(1-\varepsilon^2\nabla^2)\frac{\partial^2 u}{\partial t^2}. \tag{18}$$

Applying the operator $\partial/\partial x$ yields

$$(\lambda + 2\mu)\nabla^2 e - \alpha_1 \nabla^2 T - \alpha_2 \nabla^2 C = \rho(1 - \varepsilon^2 \nabla^2)\frac{\partial^2 e}{\partial t^2}. \tag{19}$$

The heat and diffusion equations, formulated within the framework of memory-dependent theory, are represented as follows

$$\left(1 + \ell \frac{\partial}{\partial x} + \tau_q D_{\tau_q}\right)\left(\rho\, C_e \frac{\partial T}{\partial t} + \alpha_1 T_0 \frac{\partial e}{\partial t} + a T_0 \frac{\partial C}{\partial t} - Q\right) = k\nabla^2 T, \tag{20}$$

$$(1 + \tau_\eta D_{\tau_\eta})\frac{\partial C}{\partial t} = \mathfrak{D}\,(-\alpha_2 \nabla^2 e + b\nabla^2 C - a\nabla^2 T). \tag{21}$$

In this formulation, the single-phase-lag (SPL) parameter τ_q is not treated as a standalone relaxation constant but is intrinsically embedded within the memory-dependent derivative (MDD) operator. It influences the shape and behavior of the temporal kernel function $K(t - \xi)$, which governs how past thermal states contribute to the present response. This integration allows the SPL model to modulate the memory horizon and weighting profile of the MDD framework, thereby capturing both finite-speed heat conduction and nonlocal temporal effects in a unified convolution-based structure. As a result, the delayed thermal response introduced by SPL is inherently reflected in the system's memory dynamics, ensuring a physically consistent representation of thermal inertia and wave dispersion.

3.2. Dimensionless variables

The dimensionless quantities are defined as follows

$$\begin{gathered}(x', u', \ell', \varepsilon') = c_0\eta_0\,(x, u, \ell, \varepsilon), \quad (T', C') = \frac{(\alpha_1 T, \alpha_2 C)}{\rho c_0^2}, \quad (t', \tau'_q, \tau'_\eta) = c_0^2\eta_0(t, \tau_q, \tau_\eta), \\ \sigma'_{ij} = \frac{\sigma_{ij}}{\rho c_0^2}, \quad \phi' = \frac{\phi}{\alpha_2}, \quad c_0^2 = \frac{\lambda + 2\mu}{\rho}, \quad \eta_0 = \frac{\rho C_e}{k}, \quad \mathcal{P}' = \frac{\mathcal{P}}{\mathcal{P}_0}.\end{gathered} \tag{22}$$

The governing equations can be written in dimensionless form (omitting the prime notation) as follows

$$\left(1 + \ell \frac{\partial}{\partial x} + \tau_q D_{\tau_q}\right)\left(\frac{\partial T}{\partial t} + \gamma_1 \frac{\partial e}{\partial t} + \gamma_1\gamma_2 \frac{\partial C}{\partial t} - \gamma_1\gamma_3 Q\right) = \gamma_4 \nabla^2 T, \tag{23}$$

$$(1 + \tau_\eta D_{\tau_\eta})\frac{\partial C}{\partial t} = \mathfrak{D}\eta_0\,(\gamma_5 \nabla^2 e + b\nabla^2 C + \gamma_2\gamma_5 \nabla^2 T), \tag{24}$$

$$\nabla^2 e - \nabla^2 T - \nabla^2 C = (1 - \varepsilon^2 \nabla^2)\frac{\partial^2 e}{\partial t^2}, \tag{25}$$

$$\nabla^2 \mathcal{P} - \gamma_6 \frac{\partial^2 \mathcal{P}}{\partial t^2} = \gamma_7 \frac{\partial^2 T}{\partial t^2}, \tag{26}$$

$$\phi = -e - \frac{b}{\gamma_5} C - \gamma_2 T, \tag{27}$$

$$(1 - \varepsilon^2 \nabla^2)\sigma_{xx} = e - \alpha_1 T - \alpha_2 C, \tag{28}$$

where

$$\begin{gathered}\gamma_1 = \frac{\alpha_1^2 T_0}{\rho^2 C_e c_0^2}, \quad \gamma_2 = \frac{a c_0^2 \rho}{\alpha_1 \alpha_2}, \quad \gamma_3 = \frac{1}{\alpha_1 c_0^2 \eta_0 T_0}, \\ \gamma_4 = \frac{k\eta_0}{\rho\, C_e}, \quad \gamma_5 = -\frac{\alpha_2^2}{\rho c_0^2}, \quad \gamma_6 = \frac{c_0^2}{c_s^2}, \quad \gamma_7 = \frac{\zeta\beta\rho c_0^2}{\alpha_1 P_0}.\end{gathered} \tag{29}$$

3.3. Initial and boundary conditions

The initial and boundary conditions associated with the proposed problem are as follows

$$\begin{aligned} T(x,0) = \frac{\partial T(x,0)}{\partial t} = 0, \quad u(x,0) = \frac{\partial u(x,0)}{\partial t} = 0, \\ \mathcal{P}(x,0) = \frac{\partial \mathcal{P}(x,0)}{\partial t} = 0, \quad \phi(x,0) = \frac{\partial \phi(x,0)}{\partial t} = 0. \end{aligned} \tag{30}$$

It is assumed that the system is initially at rest, with a uniform temperature T_0. The rod, with a non-dimensional length L, is fixed at both ends. It is subjected to a thermal shock at one boundary $x = 0$ while the other boundary remains thermally insulated.

$$\begin{aligned} u(0,t) = u(L,t) = 0, \quad T(0,t) = T_1 H(t), \quad \frac{\partial T(L,t)}{\partial x} = 0, \quad \phi(0,t) = \phi_1 H(t), \\ \mathcal{P}(0,t) = \mathcal{P}_1 H(t), \quad \sigma_{xx}(0,t) = \sigma_1, \end{aligned} \tag{31}$$

in which $T_1, \mathcal{P}_1\ (>0)$ are constant values and ϕ_1 is the chemical load at $x = 0$. A moving heat source with constant strength Q_0 is applied to the rod which continuously releases energy as it travels along the x-axis in a positive direction at a uniform speed λ, given as

$$Q = Q_0 H(x - \lambda t) \Rightarrow \bar{Q} = Q_0\, e^{-sx/\lambda}/s. \tag{32}$$

Here, it is assumed that the excitation frequencies lie in the MHz range, the resulting acoustic wavelengths are on the order of tens to hundreds of microns, comparable to the rod's length, thus justifying the use of nonlocal elasticity.

Wang and Li (2011) introduced the MDD formulation, demonstrating that the memory influence of any function over a sliding interval is

$$D_\tau^m Y(t) = \frac{1}{\tau} \int_{t-\tau}^{t} K(t-\xi)\, Y^m(\xi)\, \mathrm{d}\xi \quad (\tau > 0), \tag{33}$$

where the kernel $K(t-\xi)$ is defined as (Wang & Li, 2011)

$$K(t-\xi) = 1 - \frac{2p_2}{\tau_i}(t-\xi) + \frac{p_1^2}{{\tau_i}^2}(t-\xi)^2 = \begin{cases} 1-(t-\xi) & , \text{if } p_1 = 0, p_2 = \dfrac{\tau_i}{2} \\ \left(1 - \dfrac{t-\xi}{\tau_i}\right)^2 & , \text{if } p_1 = 1, p_2 = 1 \end{cases} \quad \text{for } i = q, \eta. \tag{34}$$

Here, the parameters p_1 and p_2 are coefficients that shape the memory kernel, controlling how past states influence the present.

4. SOLUTION ANALYSIS

The Laplace transform of a function $f(x,t)$ is defined as

$$\bar{f}(x,s) = L[f(x,t)] = \int_0^\infty e^{-st} f(x,t)\mathrm{d}t, \quad \mathrm{Re}(s) > 0. \tag{35}$$

Here, s is the Laplace transform variable that converts time-dependent equations into algebraic form in the complex frequency domain. Applying the Laplace transform to the memory-derivative using the convolution theorem, we obtain

$$\mathcal{L}[\tau_i D_{\tau_i}^p f(x,t)] = \mathcal{L}\left[\int_{t-\tau_i}^{t} K(t-\xi) f^p(x,\xi)\mathrm{d}\xi\right] = s^{p-1} G(s,\tau_i)\mathcal{L}\left[f(x,t)\right]. \tag{36}$$

In the Laplace domain, the kernel functions are expressed as

$$G(s,\tau_i)=\begin{cases}(1-e^{-s\tau_i})(1-1/s)+\tau_i e^{-s\tau_i}, & \text{if } p_1=0, p_2=\dfrac{\tau_i}{2}\\ \left(1-\dfrac{2}{s\,\tau_i}\right)+\dfrac{2(1-e^{-s\tau_i})}{s^2{\tau_i}^2}, & \text{if } p_1=1, p_2=1\end{cases} \tag{37}$$

Applying the Laplace transforms to Eqs. (23)–(28) and simplifying, we obtain

$$\left(\beta_1+\ell\frac{\partial}{\partial x}\right)(s\bar{T}+\gamma_1 s\,\bar{e}+\gamma_1\gamma_2 s\bar{C}-\gamma_1\gamma_3\bar{Q})=\gamma_4\nabla^2\bar{T}, \tag{38}$$

$$(\nabla^2-\beta_2)\bar{C}+\beta_3\nabla^2\bar{e}+\beta_4\nabla^2\bar{T}=0, \tag{39}$$

$$\beta_5\nabla^2(\bar{T}+\bar{C})=(\nabla^2-\beta_6)\,\bar{e}, \tag{40}$$

$$\nabla^2\bar{\mathcal{P}}-\gamma_6 s^2\bar{P}=\gamma_7 s^2\bar{T}, \tag{41}$$

$$\bar{\phi}=-\bar{e}-\frac{b}{\gamma_5}\bar{C}-\gamma_2\bar{T}, \tag{42}$$

$$(1-\varepsilon^2\nabla^2)\bar{\sigma}_{xx}=\bar{e}-\alpha_1\bar{T}-\alpha_2\bar{C}, \tag{43}$$

where

$$\beta_1=1+G(s,\tau_q),\ \beta_2=\frac{(1+\tau_\eta D_{\tau_\eta})s}{\mathfrak{D}b\eta_0},\ \beta_3=\frac{\gamma_5}{b},\ \beta_4=\beta_3\gamma_2,\ \beta_5=\frac{1}{(1+\varepsilon^2 s^2)},\ \beta_6=\beta_5 s^2.$$

Applying the elimination method to Eqs. (38)–(40)yields

$$[\mathcal{A}_1\nabla^6+\mathcal{A}_2\nabla^5+\mathcal{A}_3\nabla^4+\mathcal{A}_4\nabla^3+\mathcal{A}_5\nabla^2+\mathcal{A}_6\nabla+\mathcal{A}_7](\bar{T},\bar{e},\bar{C})=(\Omega_1,\,\Omega_2,\Omega_3)e^{-sx/\lambda}, \tag{44}$$

where

$$\begin{aligned}
\mathcal{A}_1&=\gamma_4(1+\beta_3\beta_5),\\
\mathcal{A}_2&=\ell s\left[-1+\gamma_1[(-1+\beta_4)\beta_5+\beta_4\gamma_2]+\beta_3\beta_5(-1+\gamma_1\gamma_2)\right],\\
\mathcal{A}_3&=s\beta_1\left[-1+\gamma_1[(-1+\beta_4)\beta_5+\beta_4\gamma_2]+\beta_3\beta_5(-1+\gamma_1\gamma_2)\right]-(\beta_2+\beta_6)\,\gamma_4,\\
\mathcal{A}_4&=\ell s\left[\beta_2(1+\beta_5\gamma_1)+\beta_6(1-\beta_4\gamma_1\gamma_2)\right],\\
\mathcal{A}_5&=s\beta_1\left[\beta_2(1+\beta_5\gamma_1)+\beta_6(1-\beta_4\gamma_1\gamma_2)\right]+\beta_2\beta_6\gamma_4,\\
\mathcal{A}_6&=-\ell s\beta_2\beta_6,\\
\mathcal{A}_7&=-s\beta_1\beta_2\beta_6,
\end{aligned} \tag{45}$$

and

$$\begin{aligned}
\Omega_1&=\frac{\gamma_1\gamma_3(\ell s-\beta_1\lambda)}{s\lambda}\left((1+\beta_3\,\beta_5)\,\frac{s^4}{\lambda^4}-(\beta_2+\,\beta_6)\frac{s^2}{\lambda^2}+\beta_2\,\beta_6\right)Q_0e^{-sx/\lambda},\\
\Omega_2&=\frac{-\gamma_1\gamma_3(\ell s-\beta_1\lambda)\beta_5}{s\lambda}\left((-1+\beta_4\,)\,\frac{s^4}{\lambda^4}+\beta_2\frac{s^2}{\lambda^2}\right)Q_0e^{-sx/\lambda},\\
\Omega_3&=\frac{-\gamma_1\gamma_3(\ell s-\beta_1\lambda)}{s\lambda}\left((\beta_4+\beta_3\beta_5)\,\frac{s^4}{\lambda^4}-\beta_4\beta_6\frac{s^2}{\lambda^2}\right)Q_0e^{-sx/\lambda}.
\end{aligned} \tag{46}$$

The general solution to Eq. (44) can be expressed as the sum of its complementary and particular solutions

$$(\bar{T},\bar{e},\bar{C})=C_1e^{m_1x}+C_2e^{m_2x}+C_3e^{m_3x}+C_4e^{m_4x}+C_5e^{m_5x}+C_6e^{m_6x}+\frac{(\Omega_1,\,\Omega_2,\Omega_3)\,e^{-sx/\lambda}}{\aleph}, \tag{47}$$

where

$$\aleph=\sum_{j=1}^{7}(-1)^{j+1}\,\mathcal{A}_j(s/\lambda)^{7-j}, \tag{48}$$

with C_1, C_2, C_3, C_4, C_5, and C_6 being arbitrary constants determined from the boundary conditions, and m_i $(i = 1, 2, 3, 4, 5, 6)$ representing the roots of the auxiliary equation

$$\mathcal{A}_1 m^6 + \mathcal{A}_2 m^5 + \mathcal{A}_3 m^4 + \mathcal{A}_4 m^3 + \mathcal{A}_5 m^2 + \mathcal{A}_6 m + \mathcal{A}_7 = 0. \tag{49}$$

Substituting Eq. (47) into Eqs. (41)–(43) yields acoustic pressure, chemical potential, and thermal stress, as shown below

$$\bar{\mathcal{P}} = \sum_{i=1}^{6} \frac{\gamma_7 s^2}{(m_i^2 - \gamma_6 s^2)} \left[\begin{array}{l} C_1 e^{m_1 x} + C_2 e^{m_2 x} + C_3 e^{m_3 x} + C_4 e^{m_4 x} + \\ C_5 e^{m_5 x} + C_6 e^{m_6 x} + \dfrac{\Omega_1}{\aleph} e^{-sx/\lambda} \end{array} \right], \tag{50}$$

$$\begin{aligned} \bar{\phi} = &- \left(\gamma_2 + 1 + \frac{b}{\gamma_5}\right) (C_1 e^{m_1 x} + C_2 e^{m_2 x} + C_3 e^{m_3 x} + C_4 e^{m_4 x} + C_5 e^{m_5 x} + C_6 e^{m_6 x}) \\ &- \frac{1}{\aleph} \left(\Omega_1 \gamma_2 + \Omega_2 + \frac{b}{\gamma_5} \Omega_3\right) e^{-sx/\lambda}, \end{aligned} \tag{51}$$

$$\bar{\sigma}_{xx} = (1 - \alpha_1 - \alpha_2) \sum_{i=1}^{6} \frac{\left[\begin{array}{l} C_1 e^{m_1 x} + C_2 e^{m_2 x} + C_3 e^{m_3 x} + C_4 e^{m_4 x} + C_5 e^{m_5 x} + C_6 e^{m_6 x} \\ + \dfrac{1}{\aleph} (\Omega_2 - \Omega_1 \alpha_1 - \Omega_3 \alpha_2) e^{-sx/\lambda} \end{array} \right]}{(1 - \varepsilon^2 m_i^2)}. \tag{52}$$

From Eq. (17), the displacement component can be expressed as follows

$$\bar{u} = \sum_{i=1}^{6} \frac{C_i e^{m_i x}}{m_i} - \frac{\Omega_2 \lambda e^{-sx/\lambda}}{s\aleph}. \tag{53}$$

The boundary conditions in the Laplace domain are expressed as

$$\begin{aligned} &\bar{u}(0,t) = \bar{u}(L,t) = 0, \quad \bar{T}(0,t) = T_1/s, \quad \frac{\partial \bar{T}(L,t)}{\partial x} = 0, \\ &\bar{\phi}(0,t) = \phi_1/s, \quad \bar{\mathcal{P}}(0,t) = \mathcal{P}_1/s, \quad \sigma_{xx}(0,t) = \frac{\sigma_1}{s}. \end{aligned} \tag{54}$$

Substituting Eq. (53) into the boundary conditions yields

$$\sum_{i=1}^{6} C_i = \frac{T_1}{s} - (\Omega_1/\aleph), \tag{55}$$

$$\sum_{i=1}^{6} \frac{C_i}{m_i} = \frac{\Omega_2 \lambda}{s\aleph}, \tag{56}$$

$$\sum_{i=1}^{6} \frac{C_i\, e^{m_i L}}{m_i} = \frac{\Omega_2 \lambda e^{-sL/\lambda}}{s\aleph}, \tag{57}$$

$$\left(\gamma_2 + 1 + \frac{b}{\gamma_5}\right) \sum_{i=1}^{6} C_i = -\frac{1}{\Upsilon} \left(\Omega_1 \gamma_2 + \Omega_2 + \frac{b}{\gamma_5} \Omega_3\right) - \frac{\phi_1}{s}, \tag{58}$$

$$\sum_{i=1}^{6} \left\{ \frac{\gamma_7 s^2}{(m_i^2 - \gamma_6 s^2)} \left[C_i + (\Omega_1/\aleph)\right] \right\} = \mathcal{P}_1/s, \tag{59}$$

$$\sum_{i=1}^{6} \frac{\left[C_i + \frac{1}{\aleph} (\Omega_2 - \Omega_1 \alpha_1 - \Omega_3 \alpha_2)\right]}{(1 - \varepsilon^2 m_i^2)} = \frac{\sigma_1}{(1 - \alpha_1 - \alpha_2)}. \tag{60}$$

The arbitrary constants C_i can be determined by solving the above system of linear equations.

5. NUMERICAL INVERSION OF THE LAPLACE TRANSFORMS

The inversion formula for the Laplace transform can be written as (Honig & Hirdes, 1984)

$$f(x,t) = \mathcal{L}^{-1}[f(x,t)] = \frac{1}{2\pi i}\int_{d-i\infty}^{d+i\infty} e^{st}\bar{f}(x,s)\mathrm{d}s. \tag{61}$$

Taking $s = d + iz$ in Eq. (61), one obtains

$$f(x,t) = \frac{e^{dt}}{2\pi}\int_{-\infty}^{\infty} e^{itz}\bar{f}(x,d+iz)\mathrm{d}z. \tag{62}$$

Now, taking the Fourier series expansion of the function $h(x,t) = e^{-dt}f(x,t)$ in the interval $[0,2L]$, we obtain the approximate formula truncated to a finite number N of terms, as

$$\begin{aligned} f_N(x,t) &= \frac{e^{dt}}{L}\left\{\frac{\bar{f}(x,d)}{2} + \mathrm{Re}\sum_{k=1}^{N}\left[e^{i\wp}\,\bar{f}(x,d+i\wp)\right]\right\} + E_r \\ &= \frac{1}{2}C_0 + \sum_{k=1}^{N} C_k + E_r, \end{aligned} \tag{63}$$

where $\wp = k\pi/L$, N is a finite integer, the parameter d is chosen such that $5 \le d \le 10$, and E_r is the discretization error added to produce the total approximation error

$$C_k = \frac{\exp(\mathrm{d}t)}{T}\left\{\exp\left[ik\pi t/T\bar{f}\left(x, d + i\frac{k\pi t}{T}\right)\right]\right\}. \tag{64}$$

The "Korrektur" method (Albrecht & Honig, 1977) allows a reduction of the discretization error without enlarging the truncation error. Therefore, the approximation Eq. (63) can be written as follows (Albrecht & Honig, 1977)

$$f_N(x,t) = f_N(x,t) - e^{-2dL}f_{N'}(x,2L+t), \quad N < N'. \tag{65}$$

We shall now describe the ε-algorithm that is used to accelerate the convergence of the series in Eq. (63) (Honig & Hirdes, 1984). Let $N = 2q+1$, where q is a natural number, and let $S_m = \sum_{k=1}^{m} C_k$ be the sequence of partial sums of the series in (63). We define the ε-sequence by $\varepsilon_{0,m} = 0, \varepsilon_{1,m} = S_m$ and $\varepsilon_{p+1,m} = \varepsilon_{p-1,m+1} + 1/(\varepsilon_{p,m+1} - \varepsilon_{p,m})$, $p = 1,2,3,\ldots$ It can be shown that the sequence $\varepsilon_{1,1}, \varepsilon_{3,1}, \varepsilon_{5,1}, \ldots, \varepsilon_{N,1}$ converges to $f(x,t) + E_r - C_0/2$ faster than the sequence of partial sums s_m ($m = 1,2,3,\ldots$). The actual procedure used to invert the Laplace transform consists of using Eq. (64). The value of $d = 7.5L$ is chosen.

$$f(x,t) = \frac{\ln(2)}{2}\sum_{r=1}^{n} G_i\,\bar{f}(x, i\ln(2)/t), \tag{66}$$

where $n \in \mathbb{Z}^+$ and G_r is given by (Honig & Hirdes, 1984)

$$G_r = (-1)^{r+n/2}\sum_{j=[(i+1)/2]}^{min(r,n/2)} \frac{j^{n/2}(2j)!}{(n/2-j)!j!(j-1)!(r-j)!(2j-r)!}. \tag{67}$$

To ensure numerical stability and convergence, we employed the Fourier series expansion method enhanced by the ε-algorithm. This approach refines partial sums and suppresses oscillations, particularly near discontinuities. Here, (i) a truncation parameter $N = 20$ and smoothing factor $d = 7.5$ were selected based on benchmarking studies to balance accuracy and computational efficiency. (ii) the error behavior was analyzed across $N = 5, 10, 15, 20$, showing that: (a) $N = 5$: high oscillations and error. (b) $N = 10$: improved smoothness but transient deviations. (c) $N = 15$: stable and accurate. (d) $N = 20$: nearly identical to $N = 15$, confirming convergence. These values balance convergence speed, numerical stability, and suppression of oscillations. Increasing N beyond 20 showed minimal accuracy gain but amplified round-off

sensitivity. A convergence profile is shown in Fig. 2 to benchmark solution stability across varying values of N.

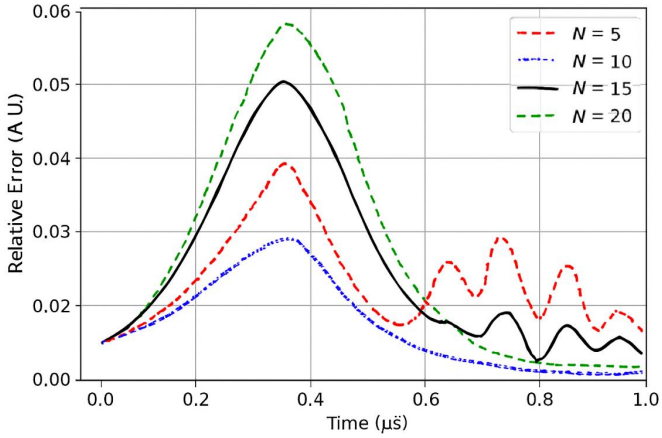

Fig. 2. Error vs. Time for four different truncation parameters

6. NUMERICAL RESULTS, DISCUSSION, AND REMARKS

This section conducts numerical computations to demonstrate the impact of the phase kernel functions, nonlocal factors, the length parameter, and diffusion phase lag attributes on the transient temperature field and its associated stress under memory-dependent derivatives. To justify the use of nonlocal elasticity, we consider a rod length of 1m and excitation frequencies in the MHz range, yielding acoustic wavelengths between 5–500 μm. This scale alignment ensures that wave propagation and structural dimensions are comparable, making size-dependent effects significant. The chosen correlation length ε captures long-range stress interactions and wave dispersion typical of microscale thermoelastic systems. The acoustic excitation frequency lies in the MHz range, and with copper's sound speed (~ 4700 m/s), the resulting acoustic wavelength ranges from 5 μm to 500 μm. These wavelengths are comparable to the rod's physical length, validating the use of nonlocal elasticity to capture scale-sensitive wave–structure interactions. In the numerical calculations, the thermoelastic material selected is copper, and the constants are (Sur, 2024)

$$\begin{gathered} k = 386\,\mathrm{W/(m\cdot K)}, \quad \alpha_t = 1.78\times 10^{-5}\,\mathrm{K^{-1}}, \quad \rho = 895\,\mathrm{kg/m^3}, \quad T_0 = 293\,\mathrm{K}, \\ C_e = 383.1\,\mathrm{J/(kg\cdot K)}, \quad \mu = 3.86\times 10^{10}\,\mathrm{Pa}, \quad \lambda = 7.76\times 10^{10}\,\mathrm{Pa}, \end{gathered} \tag{68}$$

and the other non-dimensional values for the problems are

$$\begin{gathered} \tau_q = 0.02,\ \tau_T = 0.03,\ k = 0.01, k^* = 0.2, c_0 = 0.4, \ell = 0.04, \\ \mu = 0.7, \eta = 0.5, \gamma = 0.6, \lambda = 0.85, \rho = 0.3, C_e = 0.75, K = 0.63. \end{gathered} \tag{69}$$

Dimensional values for copper's properties and excitation parameters are included to ensure that the nonlocal parameter ε reflects realistic microscale interactions. The chosen value $\varepsilon = 0.02$ corresponds to a regime where excitation wavelengths and rod dimensions are comparable, ensuring that nonlocal stress propagation is physically justified.

6.1. Impact of the nonlocal parameter

Figs. 3–8 analyze the impact of the nonlocal parameter on the changes in temperature, displacement, chemical potential, acoustic pressure, mass concentration, and nonlocal stress. Solid lines in the graphs represent local thermoelastic conditions where there is a lack of nonlocal effects, while the dashed lines illustrate the nonlocal cases that include these parameters. The

thermoelastic waves reach a steady state based on the values of the nonlocal parameters. This study provides critical insights for theoretical modeling of nonlocal thermoelasticity, which could contribute to the development of nanoscale devices. Furthermore, nonlocal effects play a key role in evaluating stress during sudden nanoscale heating scenarios.

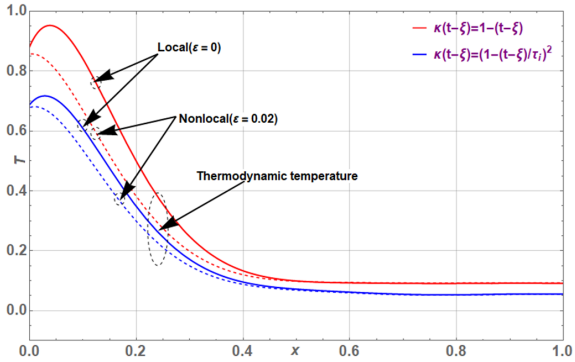

Fig. 3. Temperature (T) versus position (x) under varying kernel functions

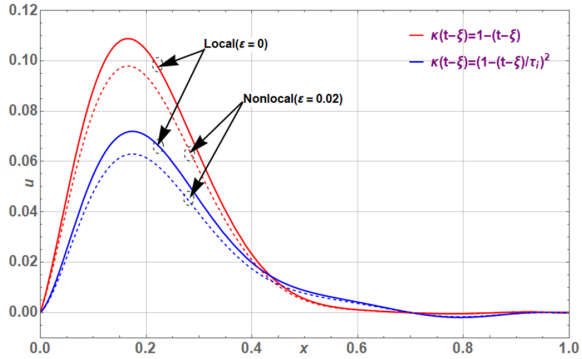

Fig. 4. Displacement (u) versus position (x) across varying kernel functions

Fig. 3 displays the thermodynamic temperature distribution along the cylindrical rod, comparing the local and nonlocal heat conduction with different memory kernel functions. The local model using a linear memory kernel shows a higher peak temperature at the application point of the heat source $(x = 0)$ and faster decay along the rod. On the other hand, the nonlocal model, which includes a quadratic kernel and a correlation length factor, shows a lower peak and a slower decay. This emphasizes the influence of nonlocal effects and memory kernels on the thermal response, leading to a lower peak temperature and a broader distribution of heat impact. The rod, constrained at both ends, is subject to thermal expansion deformation due to the applied heat source, which creates significant stress. Beyond the peak at $x = 0.15$, higher thermal nonlocal parameters lead to a larger magnitude, which satisfies the boundary conditions.

Fig. 4 compares the displacement along x for the local and nonlocal cases. In the local memory model, the linear kernel exhibits a higher peak displacement earlier, accompanied by rapid oscillations. On the other hand, the nonlocal case employing a quadratic memory kernel shows a delayed and lower peak, with fewer initial oscillations that persist over a longer distance, indicating a reduced maximum displacement and altered wave propagation and energy scattering due to nonlocal effects.

Fig. 5 illustrates that, in the case of nonlocal effects, the mass spreads more widely, resulting in a lower peak concentration near the source and a higher concentration at distant points, which represents an increased transport over longer distances. The differences are attributed to the kernel functions, with a linear kernel in the local and a quadratic kernel in the nonlocal case, which reflects the temporal effect on the mass distribution. Overall, the graph emphasizes that the nonlocal effects facilitate a wider mass spread and dampen peak concentrations.

Fig. 6 illustrates the chemical potential as a function of x for both local $(\varepsilon = 0)$ and nonlocal $(\varepsilon = 0.02)$ scenarios under linear and quadratic memory kernel functions. The chemical potential initially rises with x, reaches a peak, and then declines as x increases along the rod. In the local case, characterized by solid lines, the peaks are higher and show sharper gradients, reflecting stronger localized effects. In the nonlocal case, displayed with dashed lines, the peaks are lower, indicating the impact of nonlocal interactions that smooth and spread the chemical potential distribution over a wider region. In addition, the linear memory kernel creates more pronounced variations, while the quadratic kernel results in smoother and more gradual profiles, showing

increased retention capabilities. This comparison highlights the significant impact of nonlocal effects and kernel functions on the distribution of chemical potential.

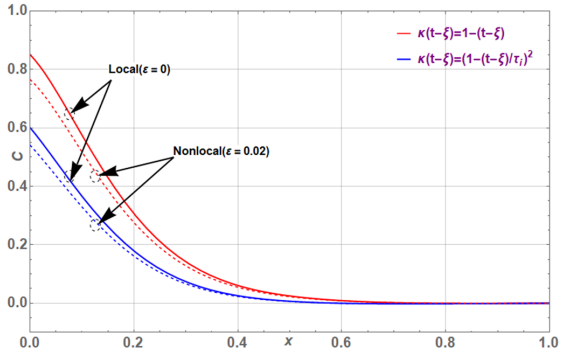

Fig. 5. Concentration (C) versus position (x) under varying kernel functions

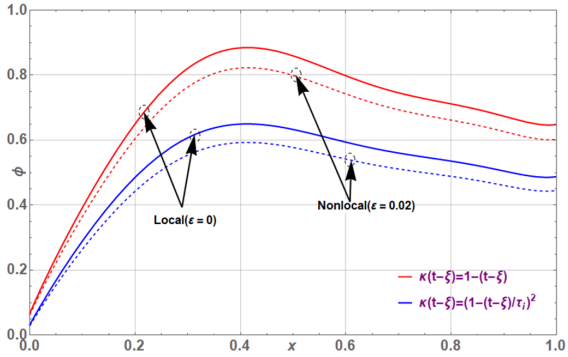

Fig. 6. Chemical potential (ϕ) versus position (x) under varying kernel functions

Fig. 7 displays the acoustic pressure along x for the local and nonlocal models with linear and quadratic memory functions. In the local case, the peak acoustic pressure values are higher and occur earlier along x, with oscillations that damp out more rapidly, reflecting stronger wave propagation. The linear kernel produces slightly higher and sharper pressure changes compared to the smoother quadratic kernel. In the nonlocal case, the acoustic pressure peaks are lower and occur later, with oscillations with smaller initial amplitudes, which persist over longer distances, indicating increased energy propagation and reduced localization. Nonlocal effects and memory kernel choice play a key role in modulating wave propagation, the intensity of maximum pressure, and oscillatory behavior, showing that material properties and memory effects control acoustic dynamics.

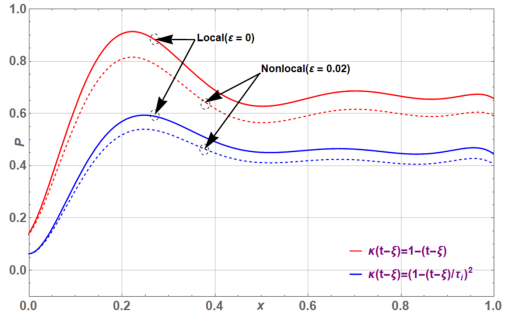

Fig. 7. Acoustic pressure $(\mathcal{P})$ versus position (x) under varying kernel functions

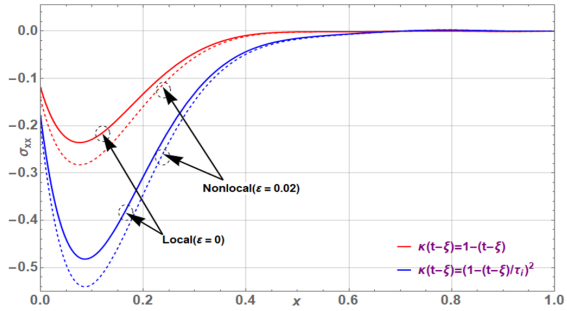

Fig. 8. Radial stress (σ_{xx}) versus position (x) under varying kernel functions

Fig. 8 shows that the nonlocal parameter affects the thermal radial stress. In the local case (solid lines), the stress values are higher and exhibit sharper variations, demonstrating stronger localized effects. For the nonlocal case (dashed lines), the stress values are lower, and the curves display smoother transitions with oscillations extending over a larger range of x, influenced by the nonlocal parameter (ε). The linear kernel leads to faster decay of stress, while the quadratic kernel retains stress gradually and emphasizes the interplay of thermal and mechanical behavior. This comparison highlights the nonlocal effects and how they influence stress dynamics along the rod. The initial negative radial stress observed in Fig. 8 arises from the convolutional structure of the MDD kernel, which amplifies early thermal gradients and induces compressive stress near the center. This is not imposed by boundary conditions but

emerges naturally from the model's temporal memory behavior. Its lowest values fall around $x \approx 0.1$ and then increase between $0.1 < x \leq 1.0$. These results confirm that nonlocal effects become prominent when excitation wavelengths approach the structural scale, validating the model's microscale relevance. To quantify the impact of kernel choice, we compared peak values for temperature, displacement, and stress. The quadratic kernel consistently reduced peak magnitudes and broadened response profiles. Table 1 summarizes the percentage reductions observed.

Table 1. Comparison of peak reductions using quadratic vs. linear memory kernels

Quantity	Linear Kernel (Peak)	Quadratic Kernel (Peak)	% Reduction
Temperature	Higher	Lower	20–30%
Displacement	Higher	Lower	15–25%
Stress	Higher, Sharper	Lower, Smoother	20–35%

6.2. Role of the correlation length parameter

The correlation parameter measures the spatial range of interactions or fluctuations in the system and plays a key role in different physical quantities. When the temperature approaches the critical point, the correlation length varies, indicating interaction over a long range. It affects the gradients of concentration, the distribution of chemical potential, and the spreading of stress in materials, shaping diffusion, phase separation, elasticity, and mechanical behavior. In addition, it affects the propagation of waves, such as acoustic pressure and displacement, and determines how these phenomena interact with the microstructure of the material. The correlation length essentially combines microscopic interactions with macroscopic properties, which is essential for understanding different systems. Figs. 9–14 show the relationship between thermodynamic properties along x under the influence of the length $\ell\ (= 0.03, 0.04, 0.05)$, with the nonlocal effect $\varepsilon = 0.02$. The red and blue curves correspond to the linear kernel $K(t-\xi) = 1-(t-\xi)$ and the quadratic kernel $K(t-\xi) = [1-(t-\xi)/\tau_i]^2$, respectively, showing that these models shape the behavior.

Fig. 9 illustrates the thermodynamic temperature along x for both linear and quadratic kernels, with the nonlocal case further exploring the impact of the length parameter. In both scenarios, a certain temperature profile reveals that increasing the length parameter leads to a higher peak temperature near the heat source and a faster decay along the length of the rod. This indicates that a larger ℓ, implying a greater range of interactions, concentrates the heat more locally, whereas a smaller ℓ results in a broader distribution of temperature.

Fig. 10 demonstrates that displacement varies spatially along the x-axis while accounting for the material's nonlocal properties. The length parameter, taking values $\ell\ (= 0.03, 0.04, 0.05)$, governs the extent to which the displacement at one point is influenced by neighboring points or even more distant points. For a larger ℓ, the displacement is more influenced by neighbouring regions. As ℓ decreases, the nonlocal effects become more pronounced, and the displacement shows a stronger interdependence with more distant areas in the material. With nonlocality incorporated , the graph reveals that displacement is not only a function of the immediate surroundings but also of wider interactions in the system. This interplay between these thermoelastic properties allows engineers and scientists to predict and optimize material behavior in applications such as wave mechanics, stress, and structural reaction analysis, especially at the micro-level and nanoscales.

Fig. 11 illustrates that the concentration C decreases with increasing x under varying conditions, as dictated by the two models and the different length parameters. Larger ℓ curves decay faster, reflecting stronger localized control, whereas smaller ℓ curves have a slower and smoother decay, reflecting the system's nonlocal interactions.

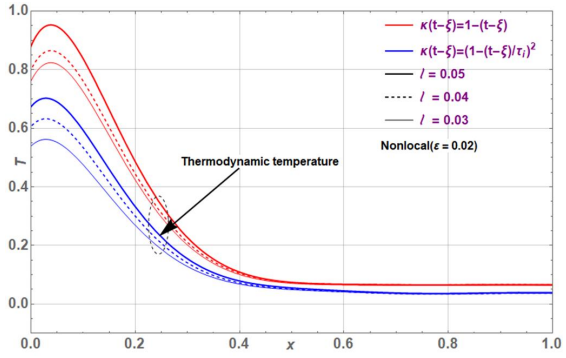

Fig. 9. Temperature (T) versus position (x) under varying length parameters

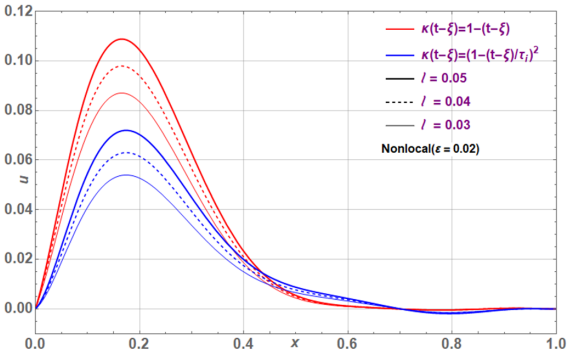

Fig. 10. Displacement (u) versus position (x) under varying length parameters

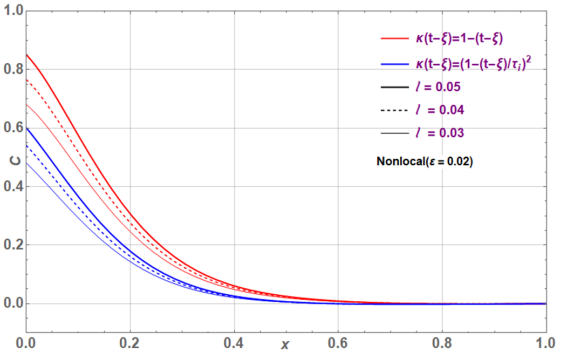

Fig. 11. Concentration (C) versus position (x) under varying length parameters

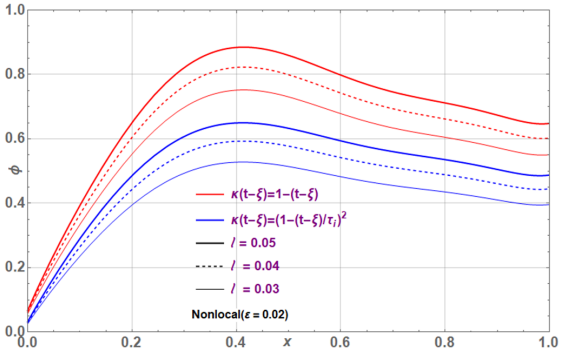

Fig. 12. Chemical potential ϕ versus position (x) under varying length parameters

The graph of chemical potential versus x demonstrates how the potential changes spatially based on the length parameter, as shown in Fig. 12. The potential increases from the origin to the maximum value and then decreases. For larger ℓ, the peak is closer to $x = 0.4$, which shows sharper gradients. For smaller ℓ, the peak moves further along the x-axis, reflecting smoother transitions due to nonlocal interactions. This behavior emphasizes the balance between local and nonlocal effects in determining potential distribution.

Fig. 13 illustrates the spatial changes in acoustic pressure, influenced by the length parameter and the kernel models. The pressure increases from $x = 0$, reaches a peak near $x = 0.2$, and then gradually decreases. This graph is key to understanding wave propagation and pressure distribution in a nonlocal medium.

Fig. 14 illustrates the length parameter's impact on the stress distribution. Initially, the stress decreases from $x = 0$ to its compressive peak, showcasing the material's reaction to nonlocal interactions. Beyond this point, the stress gradually rises and approaches zero as x nears 1, demonstrating the progression of the stress profile under these conditions. In this model, the correlation length ℓ modulates the temporal memory kernel, not spatial diffusion. A larger ℓ intensifies the system's sensitivity to recent thermal input, leading to more localized heat concentration near the source. This contrasts with spatial nonlocal models, where larger correlation lengths imply broader influence.

Finally, Figs. 3–14 already qualitatively distinguish the linear and quadratic memory kernels; we now quantify these differences. The quadratic kernel reduces the peak temperature by about 20–30%, displacement by 15–25%, and stress by 20–35% compared to the linear kernel. This

demonstrates that the quadratic kernel effectively dampens localized peaks, leading to smoother wave propagation and more stable thermoelastic behavior.

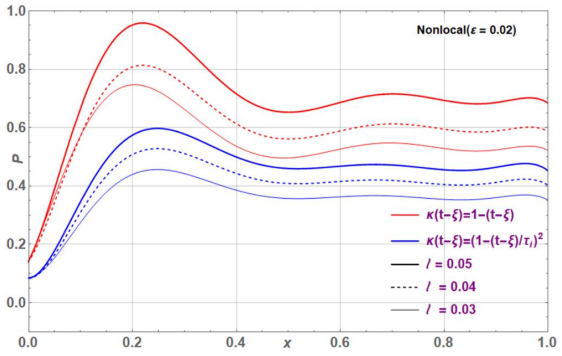

Fig. 13. Acoustic pressure ($\mathcal{P}$) versus position (x) under varying length parameters

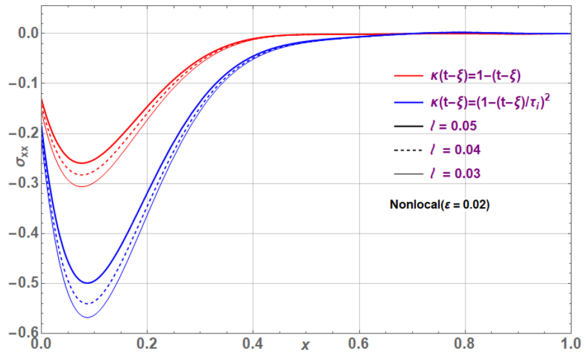

Fig. 14. σ_{xx} vs. x under different length parameters

6.3. Validation

To validate the proposed quadratic memory-dependent derivative (MDD) formulation, we benchmark our temperature profile against the nonlocal thermodiffusion model presented by Sur (2024). Both models employ copper as the thermoelastic medium and utilize a quadratic MDD kernel of the form $K(t-\xi) = \left(1 - \dfrac{t-\xi}{\tau}\right)^2$, with the memory width fixed at $\tau = 1.0$, $\varepsilon = 0.02$, and $\ell = 0.04$ to ensure consistency. A moving Heaviside-type heat source $Q(x,t) = Q_0 H(x - \lambda t)$ is applied in both cases, and temperature distributions are evaluated at the time slice $t = 0.5$ over the spatial domain $x \in [0,1]$. To align our model with Sur (2024), we converted the Moore–Gibson–Thompson (MGT) damping term to the SPL model, and retained only the kernel-driven memory structure. This requires modifying our Laplace-domain temperature equation to exclude exponential relaxation and match the pure kernel-weighted form used by Sur (2024).

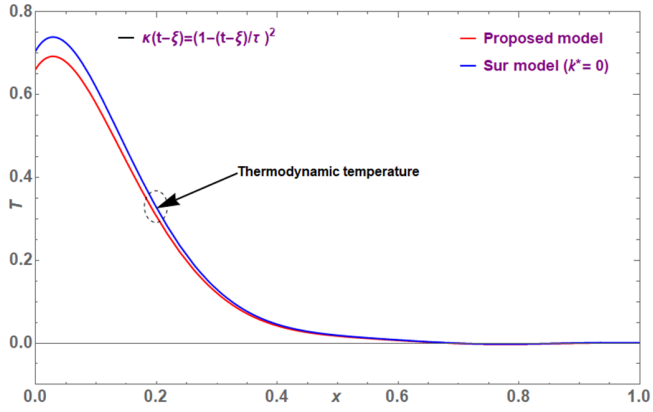

Fig. 15. Temperature profile comparison: Proposed vs published (Sur, 2024) ($k^* = 0$) model

The numerical inversion is performed using a Fourier series expansion accelerated via the ε-algorithm, while Sur's model uses a Riemann sum approach. The resulting temperature profiles exhibit near-identical peak localization near ≈ 0.05, smooth decay toward $x = 1.0$, and consistent tail behavior. This agreement confirms that the quadratic MDD kernel alone governs the thermal response and validates the physical fidelity of our formulation. Moreover, the

present model generalizes Sur's by embedding the kernel into a nonlocal operator and enabling simultaneous access to acoustic, chemical, and mechanical fields. As shown in Fig. 15, the temperature profiles over the domain $x \in [0, 1]$ exhibit consistent peak localization and smooth decay, validating the kernel-driven thermal response in both formulations.

Although the temperature comparison with Sur (2024) confirms the accuracy of our kernel-driven thermal response, full-field validation for stress, displacement, and acoustic pressure remains an open challenge due to the absence of analytical benchmarks. Future work will aim to address this gap as suitable reference models emerge.

7. CONCLUSION

This study develops a thermoacoustic framework for cylindrical rods by integrating memory-dependent derivatives (MDD), nonlocal elasticity, and single-phase-lag (SPL) heat conduction. Using Laplace-domain analysis and Fourier series inversion, the model captures coupled thermal and mechanical responses under a moving heat source. Numerical results show that kernel type and nonlocal parameters significantly affect temperature, stress, displacement, chemical potential, and acoustic pressure. Quadratic kernels produce smoother, broader, and less intense responses than linear ones, while nonlocality dampens amplitudes and prolongs oscillations. The correlation length offers tunable control over localized versus distributed behavior. These findings support the use of nonlocal and memory-based models in microscale thermal-acoustic systems and suggest applications in smart materials, sensors, and energy devices. While thermal validation has been achieved, mechanical benchmarking is limited by the current lack of kernel-based reference solutions. Expanding validation to stress and displacement fields remains a priority for future research.

DECLARATION OF COMPETING INTEREST

The authors declare that they have no known competing financial interests or personal relationships that could have appeared to influence the work reported in this paper.

CREDIT AUTHOR STATEMENT

Jitrndra Patil: *Conceptualization, Methodology*. Chandrakant Jadhav: *Supervision, Validation*. Nitin Chandel: *Conceptualization, Methodology, Formal analysis, Writing – original draft, Writing – review & editing*. Vinod Varghese: *Conceptualization*.

FUNDING

This research received no specific grant from any funding agency in the public, commercial, or not-for-profit sectors.

REFERENCES

Abouelregal, A. E. (2024). A non-local fractional two-phase delay thermoelastic model for a solid half-space whose properties change with temperature and affected by hydrostatic pressure. *ZAMM - Journal of Applied Mathematics and Mechanics / Zeitschrift für Angewandte Mathematik und Mechanik*, *104*(8), 827–838. https://doi.org/10.1002/zamm.202400102

Abouelregal, A. E., Askar, S. S., Marin, M., & Badahiould, M. (2023). The theory of thermoelasticity with a memory-dependent dynamic response for a thermo-piezoelectric functionally graded rotating rod. *Scientific Reports*, *13*(1), 9052. https://doi.org/10.1038/s41598-023-36371-2

Albrecht, P., & Honig, G. (1977). Die numerische inversion der laplace-transformierten. *Angewandte Informatik*, *8*, 336–345.

Atangana, A., & Gómez-Aguilar, J. F. (2018). Numerical approximation of riemann-liouville definition of fractional derivative: From riemann-liouville to atangana-baleanu. *Numerical Methods for Partial Differential Equations*, *34*(5), 1502–1523. https://doi.org/10.1002/num.22195

Atta, D., Abouelregal, A. E., Sedighi, H. M., & Alharb, R. A. (2024). Thermodiffusion interactions in a homogeneous spherical shell based on the modified Moore-Gibson-Thompson theory with two time delays. *Mechanics of Time-Dependent Materials*, *28*(2), 617–638. https://doi.org/10.1007/s11043-023-09598-9

Balwir, A., Kamdi, D., & Varghese, V. (2024). Memory response in quasi-static thermoelastic stress in a rod due to distributed time-dependent heat sources. *Multidiscipline Modeling in Materials and Structures*, *20*(6), 1284–1306. https://doi.org/10.1108/mmms-06-2024-0158

Barretta, R., de Sciarra, F. M., & Vaccaro, M. S. (2023). Nonlocal elasticity for nanostructures: A review of recent achievements. *Encyclopedia*, *3*(1), 279–310. https://doi.org/10.3390/encyclopedia3010018

Biot, M. A. (1956). Thermoelasticity and irreversible thermodynamics. *Journal of Applied Physics*, *27*(3), 240–253. https://doi.org/10.1063/1.1722351

Borino, G., Di Paola, M., & Zingales, M. (2011). A non-local model of fractional heat conduction in rigid bodies. *The European Physical Journal Special Topics*, *193*(1), 173–184. https://doi.org/10.1140/epjst/e2011-01389-y

Cattaneo, C. (1958). Sur une forme de l'equation de la chaleur eliminant le paradoxe d'une propagation instantanee. *Comptes Rendus de l'Académie des Sciences*, *247*, 431–433.

Chandel, N., Khalsa, L., Abouelregal, A. E., Varghese, V., & Dhore, N. (2025). Photothermal diffusion in nonsimple semiconductor strips: Impact of moving heat sources and acoustic pressure via memory and nonlocality effects. *ZAMM - Journal of Applied Mathematics and Mechanics / Zeitschrift für Angewandte Mathematik und Mechanik*, *105*(5). https://doi.org/10.1002/zamm.70061

Chandel, N., Khalsa, L., & Varghese, V. (2025). Non-simple thermoelastic diffusion interaction in a half-space with nonlocality and memory effect. *Journal of Thermal Stresses*, *48*(3), 292–318. https://doi.org/10.1080/01495739.2024.2449067

Chandel, N., Khalsa, L., Varghese, V., & Yadav, A. K. (2024). Nonlocal thermoelastic analysis of a spherically symmetric elastic sphere with memory effects. *Mechanics of Advanced Materials and Structures*, *32*(21), 5330–5342. https://doi.org/10.1080/15376494.2024.2422575

Dhore, N., Khalsa, L., & Varghese, V. (2025). Hygrothermoelastic analysis of the nano-circular plate with memory effect. *Applied Mathematical Modelling*, *138*, 115797. https://doi.org/10.1016/j.apm.2024.115797

El-Dali, A., Othman, M. I. A., Gamal, E. M., & Alkhatib, S. (2024). Impact of the eigenvalue approach on the model of moore-gibson-thompson during photo-acoustic semiconducting excitation. *Springer Nature Preprint*. https://doi.org/10.21203/rs.3.rs-5300313/v1

Eringen, A. C. (1974a). Memory dependent nonlocal elastic solids. *Letters in Applied Engineering Sciences*, *2*(3), 145–159.

Eringen, A. C. (1974b). Theory of nonlocal thermoelasticity. *International Journal of Engineering Science*, *12*(12), 1063–1077. https://doi.org/10.1016/0020-7225(74)90033-0

Eringen, A. C. (1984). Plane waves in nonlocal micropolar elasticity. *International Journal of Engineering Science*, *22*(8–10), 1113–1121. https://doi.org/10.1016/0020-7225(84)90112-5

Eringen, A. C., & Edelen, D. G. B. (1972). On nonlocal elasticity. *International Journal of Engineering Science*, *10*(3), 233–248. https://doi.org/10.1016/0020-7225(72)90039-0

Ezzat, M. A., El-Karamany, A. S., & El-Bary, A. A. (2015). A novel magneto-thermoelasticity theory with memory-dependent derivative. *Journal of Electromagnetic Waves and Applications*, *29*(8), 1018–1031. https://doi.org/10.1080/09205071.2015.1027795

Ezzat, M. A., El-Karamany, A. S., & El-Bary, A. A. (2016). Electro-thermoelasticity theory with memory-dependent derivative heat transfer. *International Journal of Engineering Science*, *99*, 22–38. https://doi.org/10.1016/j.ijengsci.2015.10.011

Furati, K. M., Kassim, M. D., & Tatar, N. T. (2012). Existence and uniqueness for a problem involving hilfer fractional derivative. *Computers and Mathematics with Applications*, *64*(6), 1616–1626. https://doi.org/10.1016/j.camwa.2012.01.009

Galucio, C., Deu, J. F., & Ohayon, R. (2004). Finite element formulation of viscoelastic sandwich beams using fractional derivative operators. *Computational Mechanics*, *33*(4), 282–291. https://doi.org/10.1007/s00466-003-0529-x

Ghavanloo, E., Rafii-Tabar, H., & Fazelzadeh, S. A. (2019). Recent developments and future challenges in the application of nonlocal elasticity theory. In *Computational continuum mechanics of nanoscopic structures* (pp. 261–275). Springer International Publishing. https://doi.org/10.1007/978-3-030-11650-7_12

Honig, G., & Hirdes, U. (1984). A method for the numerical inversion of laplace transforms. *Journal of Computational and Applied Mathematics*, *10*(1), 113–132. https://doi.org/10.1016/0377-0427(84)90075-x

Jesus, I. S., & Machado, J. A. T. (2009). Implementation of fractional-order electromagnetic potential through a genetic algorithm. *Communications in Nonlinear Science and Numerical Simulation*, *14*(5), 1838–1843. https://doi.org/10.1016/j.cnsns.2008.08.015

Kilbas, A., Srivastava, H. M., & Trujillo, J. J. (2006). *Theory and applications of fractional differential equations*. Elsevier.

Lazar, M., & Agiasofitou, E. (2022). Nonlocal elasticity of klein–gordon type: Fundamentals and wave propagation. *Wave Motion*, *114*, 103038. https://doi.org/10.1016/j.wavemoti.2022.103038

Lord, H. W., & Shulman, Y. (1967). A generalized dynamical theory of thermoelasticity. *Journal of the Mechanics and Physics of Solids*, *15*(5), 299–309. https://doi.org/10.1016/0022-5096(67)90024-5

Mainardi, F. (1996). Fractional relaxation-oscillation and fractional diffusion-wave phenomena. *Chaos, Solitons and Fractals*, *7*(9), 1461–1477. https://doi.org/10.1016/0960-0779(95)00125-5

Meral, F. C., Royston, T. J., & Magin, R. (2010). Fractional calculus in viscoelasticity: An experimental study. *Communications in Nonlinear Science and Numerical Simulation*, *15*(4), 939–945. https://doi.org/10.1016/j.cnsns.2009.05.004

Miller, K. S., & Ross, B. (1993). *An introduction to the fractional calculus and fractional differential equations*. John Wiley; Sons.

Mondal, S. (2020). Memory response in a magneto-thermoelastic rod with moving heat source based on eringen's nonlocal theory under dual-phase lag heat conduction. *International Journal of Computational Methods*, *17*(9), 1950072. https://doi.org/10.1142/s0219876219500725

Podlubny, I. (1990). *Fractional differential equations*. Academic Press.

Raddadi, M. H., Lotfy, K., El-Bary, A. A., Mahdy, A. M. S., & Elidy, E. S. (2025). A novel model of photoacoustic and thermalelectronic waves in semiconductor material. *AIP Advances*, *15*(1). https://doi.org/10.1063/5.0236367

Said, S. M. (2022). 2d problem of nonlocal rotating thermoelastic half-space with memory-dependent derivative. *Multidiscipline Modeling in Materials and Structures*, *18*(2), 339–350. https://doi.org/10.1108/mmms-01-2022-0011

Shakeriaski, F., Ghodrat, M., Escobedo-Diaz, J., & Behnia, M. (2021). Recent advances in generalized thermoelasticity theory and the modified models: A review. *Journal of Computational Design and Engineering*, *8*(1), 15–35. https://doi.org/10.1093/jcde/qwaa082

Sur, A. (2024). Elasto-thermodiffusion in a slim strip revisited with new definition of nonlocal heat conduction. *International Journal of Applied and Computational Mathematics*, *10*(6), 159. https://doi.org/10.1007/s40819-024-01775-9

Tzou, D. Y. (2014, September). *Macro- to microscale heat transfer: The lagging behavior*. John Wiley; Sons. https://doi.org/10.1002/9781118818275

Veeresha, P., Prakasha, D. G., & Baskonus, H. M. (2019). New numerical surfaces to the mathematical model of cancer chemotherapy effect in caputo fractional derivatives. *Chaos: An Interdisciplinary Journal of Nonlinear Science*, *29*(1), 013119. https://doi.org/10.1063/1.5074099

Vernotte, P. (1958). Les paradoxes de la théorie continue de l'équation de la chaleur. *Comptes Rendus de l'Académie des Sciences*, *246*, 3154–3155.

Wang, J. L., & Li, H. F. (2011). Surpassing the fractional derivative: Concept of the memory-dependent derivative. *Computers and Mathematics with Applications*, *62*(3), 1562–1567. https://doi.org/10.1016/j.camwa.2011.04.028

Yu, Y. J., Hu, W., & Tian, X. G. (2014). A novel generalized thermoelasticity model based on memory-dependent derivative. *International Journal of Engineering Science*, *81*, 123–134. https://doi.org/10.1016/j.ijengsci.2014.04.014